Chapter

Swept-Source Optical Coherence Tomography and Optical Coherence Tomography Angiography in Selected Posterior Uveitides

Magdy Moussa and Mahmoud Leila

Abstract

The pathogenesis of uveitis entails changes in the structural morphology of the macula, choroid, and choroidal perfusion. Documentation of these pathologic alterations is pivotal in making a proper diagnosis and in follow-up of outcomes of therapy. The newly-introduced swept-source optical coherence tomography (SS-OCT) and optical coherence tomography angiography (SS-OCTA) were harbingers of a whole new era of noninvasive in vivo layer-to-layer dissection of macular and choroidal structural changes in uveitis and of disease-related vascular profile patterns. This new information unraveled new aspects of the underlying pathogenetic mechanisms in different uveitides and added to our understanding of the disease process. Monitoring choroidal thickness was introduced as a novel sensitive index for evaluation and titration of treatment response. Moreover, the ensuing complications of uveitis as poor pupillary dilatation due to posterior synechiae and mild to moderate opacities due to cataract or vitritis that frequently posed pertinacious impediments for reproducible imaging were overcome by SS-OCT features notably long-wavelength scanning laser and reduced sensitivity roll-off features. In the current manuscript we present our experience in diagnosis and management of selected posterior uveitides using SS-OCT and SS-OCTA.

Keywords: swept-source OCT in uveitis, swept-source OCTA in uveitis, Vogt-Koyanagi-Harada, serpiginous choroiditis, multifocal choroiditis, punctate inner choroidopathy, toxoplasmosis

1. Introduction

Traditionally, management of posterior segment inflammation secondary to uveitis relied on fundus fluorescein angiography (FFA) and indocyanine green angiography (ICG) for assessment of the pathological alteration of the inner- and outer-blood-retina-barriers (BRB), disturbances in choroidal perfusion, and the structural sequelae of inflammation in the macular area and elsewhere in the retina and the choroid [1, 2]. These tests offered indirect biological clues to evaluate the quality of the retinal and choroidal circulations in terms of patterns of leakage and grades of perfusion; henceforth, determination of disease evolution through remissions and exacerbations, titration of posology and monitoring tissue response to therapy [3, 4].

1.1 Limitations of conventional angiographic modalities

Despite the invaluable input of these diagnostic tools, they had inherent limitations that posed major impediment to full exploration of the pathological events in the posterior segment secondary to different uveitides. Firstly, the profuse leakage of the sodium fluorescein molecule from the choriocapillaris, and the optical scattering of incident light by the retinal nerve fiber layer confined the utility of FFA mostly to single-layered evaluation of the pathological cascade of events developing at the level of superficial capillary plexus (SCP) and left the observer with vague deductions regarding the ongoing pathology in the deep capillary plexus (DCP), the choriocapillaris and the choroidal stroma [5–9]. Secondly, the inflammatory by-products of uveitides and the associated pathological features included intra-, sub-retinal and sub-retinal pigment epithelium (RPE) fluid and/or lipoproteinaceous deposits, sub-retinal and sub-RPE fibrosis, RPE thickening and pigment epithelial detachment (PED). These features shared common FFA leakage and ICG fluorescence properties among themselves and with choroidal neovascular membrane (CNV) that might complicate posterior segment inflammation, which made these entities virtually indistinguishable from each other and subsequently delayed diagnosis and prompt intervention for treating CNV. Thirdly, the longevity of uveitis disease process and its propensity to undulating course of remissions and exacerbations render repetitive dye-based FFA and ICG angiography impractical and even hazardous in routine clinical practice due to their invasive nature [3, 4, 10].

1.2 Swept-source optical coherence tomography (SS-OCT) and optical coherence tomography angiography (SS-OCTA) technology: novel imaging modality in uveitides

The introduction of swept-source optical coherence tomography (SS-OCT) technology revolutionized imaging of ocular posterior segment in uveitides and circumvented several classical obstacles that long represented significant hindrance to correct diagnosis. Firstly, SS-OCT employed a long wavelength laser source (1050 nm) operating at an ultra-high scanning speed (100.000 A-scan/second). The tandem of ultra-high-speed image acquisition, laser beam collimation and reduced sensitivity roll-off feature helped defraying scattering of the scanning light as it traveled through the retina, with subsequent rendition of ultra-high-definition images of retinal layers quasi-in-vivo histological tissue dissection [11, 12]

Moreover, these features enhanced beam penetration in media opacities and poorly dilatable pupils, which are common features associated with uveitis and that pose significant impediment to interpretable images. New morphological changes in the vitreo-retinal interface, the retina, the choroidal layers, and changes in choroidal thickness secondary to uveitides were unveiled and employed as biomarkers for diagnosis of uveitis, detection of ensuing complications and monitoring disease progression and response to therapy. Secondly, superior axial resolution and greater depth of penetration of the incident beam in enhanced depth (EDI)- and SS-OCT imaging allowed simultaneous documentation of pathological changes in the vitreous, vitreo-retinal interface, retina, and choroid in a single frame amenable to scrutiny and exploration of the true magnitude of tissue involvement by the disease process [13–18].

Thirdly, SS-OCT incorporated a blood flow detection algorithm; OCTARA (Optical Coherence Tomography Angiography Ratio Analysis). This novel feature allowed evaluation of the retinal vascular plexuses and of the choriocapillaris that are frequently targeted in uveitides. The algorithm relies on decorrelation motion contrast between rapidly repeated SS-OCT B-scans to visualize blood flow in vivo without the need for contrast injection. This OCTA implement benefits from being

merged with SS-OCT technology to generate separate en-face images of the retinal SCP, DCP, and the choriocapillaris. It is worthy of note that OCTARA algorithm generates OCTA images by registering B-scan repetition at each scan location then computing a ratio-based result between corresponding image pixels. This method preserves the integrity of the OCT spectrum and does not result in compromised axial resolution, an inherent disadvantage of other OCTA technologies [19–22].

OCTA excelled in delineating inflammatory CNV that could complicate posterior uveitis and determining its state whether active, quiescent, or recurrent based on the neovascular network morphological criteria [10, 23, 24]. Inflammatory CNV has long posed a diagnostic predicament in the past due to overlapping leakage and/or fluorescence patterns with non-neovascular inflammatory tissue on FFA and ICG, respectively. Likewise, CNV and non-neovascular inflammatory lesions frequently exhibit similar light backscattering properties that render them indistinguishable from each other on structural OCT [3, 4, 25, 26].

It is worthy of note that OCTA does not provide information on vascular leakage, which is a crucial index of the integrity of the inner BRB in cases of vasculitis associated with uveitides. In cases of active vasculitis, OCTA could be even misleading as the leakage of plasma from a disrupted inner BRB into the extra-cellular compartment might slow-down the blood stream velocity well below the detection threshold of OCTA, which might be falsely interpreted by OCTA as reduced vessel density and capillary non-perfusion [3].

2. Authors' case presentations

In the following case presentations, we present our experience with SS-OCT and SS-OCTA using the swept-source DRI OCT Triton machine version 10.11 (Topcon Corporation, Tokyo, Japan) and the OCTARA algorithm (Topcon Corporation, Tokyo, Japan), respectively, in imaging common non-infectious and infectious uveitides, with emphasis on the importance of multi-modal imaging approach in which different imaging modalities complement one another to reveal the true extent of the ongoing pathology.

2.1 Non-infectious uveitides

2.1.1 Vogt-Koyanagi-Harada (VKH)

VKH is a multi-system disorder featuring ocular, auditory, integumentary, and neurological manifestations. Ocular involvement in VKH is in the form of bilateral granulomatous panuveitis that is notorious of profound drop of vision, hence the need for early aggressive treatment. Posterior segment involvement in the acute stage comprises diffuse choroiditis, optic disc hyperemia, multifocal serous retinal detachment or bullous exudative retinal detachment. As the chronic stage of the disease ensues, the patient develops ocular depigmentation in the form of chorioretinal depigmented scars and retinal pigmentary disturbances [27, 28].

The primary target tissue in VKH is the choroidal stroma which endures dense infiltration with inflammatory cells and subsequent thickening due to engorgement of choroidal vessels and serous exudation. Eventually, the RPE dehisces giving way to the inflammatory infiltrates and serous fluid into the sub-retinal space. RPE folds develop due to displacement by the thickened choroid. The choriocapillaris undergoes ischemic changes especially in recurrent cases in the form of localized vascular loss. This could be explained by severe hypoperfusion secondary to inflammation or by pressure atrophy from inflammatory granulomas

[29, 30]. These areas of choriocapillaris loss appear on OCTA examination as sharply demarcated flow-voids that might recover after resolution of inflammation [31, 32]. Recurrent attacks of inflammation with subsequent breaching of the RPE-Bruch's complex could trigger CNV formation. In that context OCTA helps differentiating CNV from inflammatory tissue by demonstrating the hyperintense signal characteristic of CNV formation in the outer retina slab [3, 4].

2.1.1.1 Case presentation

A 58-year-old male presenting with bilateral diminution of vision of approximately 3 months duration. The patient reported more severe drop of vision in the left eye. He had history of previous similar attacks of visual disturbances in both eyes. His best-corrected visual acuity (BCVA) was 6/60 and 1/60 in the right and left eyes, respectively. Fundus examination of the right eye revealed multifocal serous retinal detachment in the posterior pole along with extensive sub-retinal exudate formation and optic nerve head (ONH) hyperemia. FFA revealed multiple leaking points at the level of the RPE with pooling of dye into the sub-retinal space and hyperfluorescence of the ONH due to leakage from dilated optic disc vessels. Fundus examination of the left eye showed similar findings in the posterior pole in addition to a sub-macular greenish-yellow lesion that demonstrated early hyperfluorescence with minimal leakage and late staining suggestive of predominantly scarred CNV.

2.1.1.1.1 SS-OCT and SS-OCTA features

The corresponding SS-OCT scan of the right eye showed marked thickening of the choroid with secondary undulations of the overlying RPE layer. The sub-retinal space showed multiple loculi of serous fluid and complete disruption of the

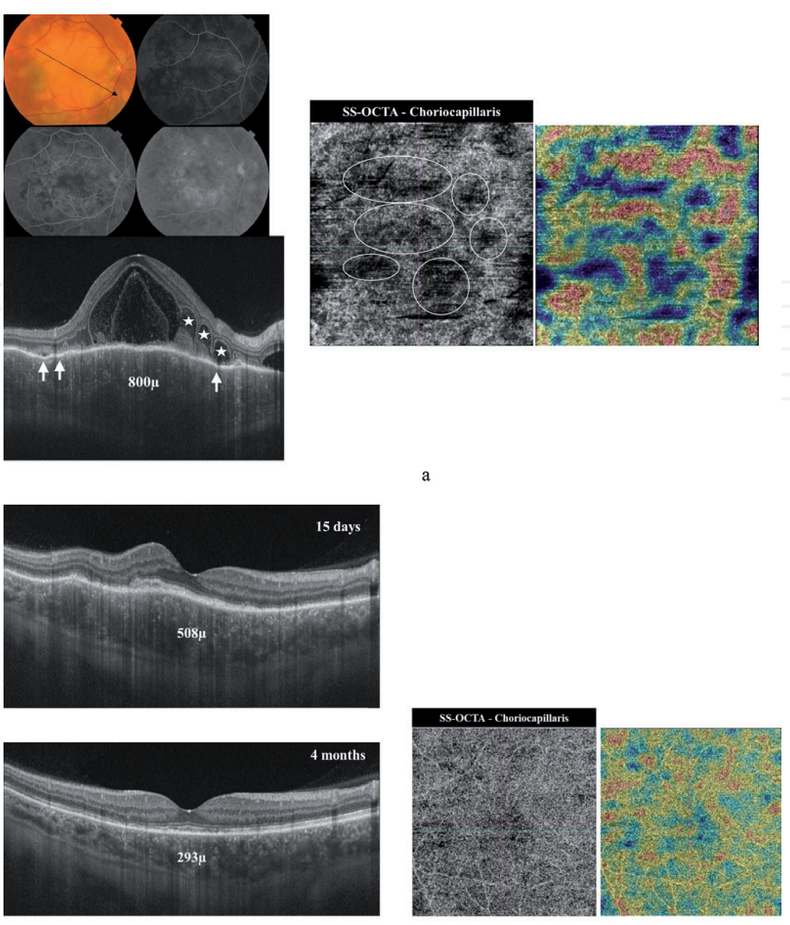

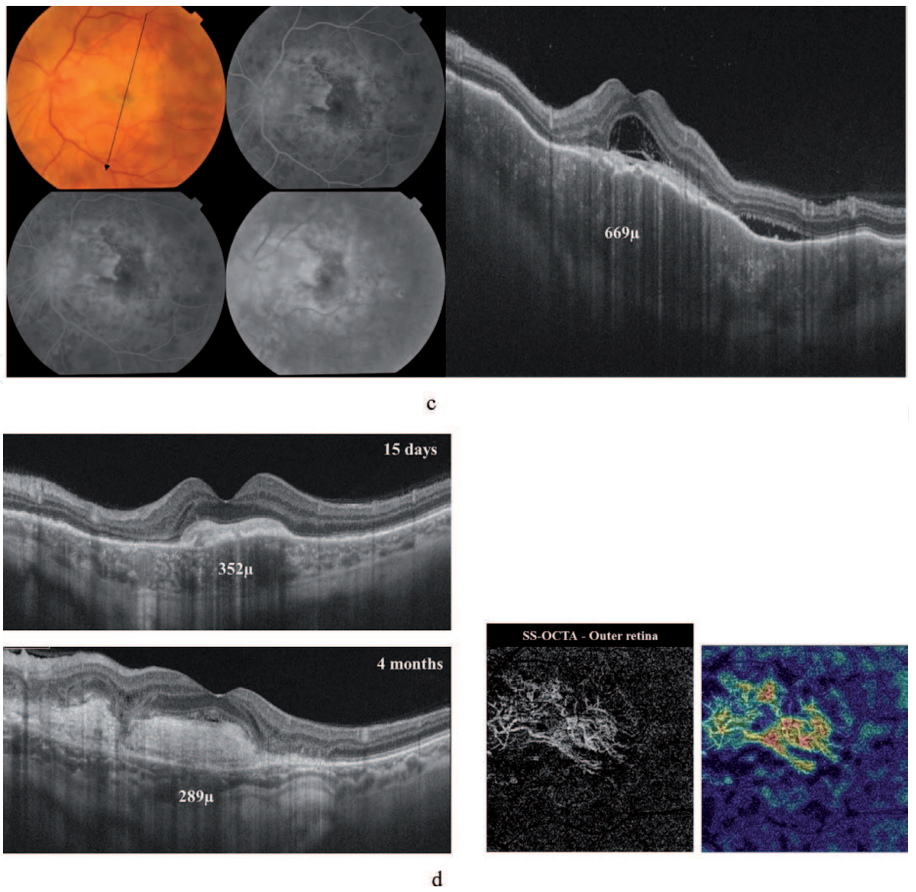

Figure 1.
(A) Top left: Color fundus photo and FFA of the right eye of a 58-year-old man presenting with acute attack of VKH. The posterior pole has a creamy yellowish appearance due to combination of multifocal neurosensory detachment and sub-retinal deposition of serous exudates. The ONH is hyperemic. FFA shows patchy choroidal filling persisting well into the venous phase, along with multiple pin-point leakage at the level of the RPE and diffuse hyperfluorescence due to pooling of dye into localized areas of neurosensory detachment. Bottom left: Radial scan SS-OCT shows marked increase in choroidal thickening (800 μm) and engorged choroidal vessels. Note the difficult delineation of the choroidal-scleral interface (CSI) due to optical hyporeflectivity secondary to engorged choroid. There are innumerable hyperreflective dots scattered within the choroid and possibly represent cellular inflammatory aggregates. The RPE shows multiple folds (white arrows). The neurosensory retina shows multiple hyporeflective loci separated by hyperreflective tissue septa (asterisks). Central macular thickness (CMT) is 970 μm. The hyporeflective loci are filled with hyperreflective amorphous material. There is complete disruption of the ellipsoid zone and outer retinal layers. Right: En-face SS-OCTA image of the choriocapillaris in a 6 × 6 mm field. Note the multiple discrete hypointense flow voids that are scattered within the choriocapillaris layer (white circles). The corresponding flow-density map shows blue color shades corresponding to the flow-void areas and denoting marked reduction of vessel density. (B) Radial scan SS-OCT images of the same patient at 15 days and 4 months after high-dose systemic steroid treatment. Note complete resolution of neurosensory detachment, and restoration of the ellipsoid zone. There is residual thickening of the RPE. Note improved delineation of the CSI and progressive disappearance of the previously seen hyperreflective dots in the choroid with resolution of choroidal inflammation. Bottom right: En-face SS-OCTA image of the choriocapillaris in a 6 × 6 mm field and the corresponding flow-density map at 4-month follow-up visit show significant recovery of the normal texture of the choriocapillaris denoting improvement of choriocapillaris perfusion. (C) Left: Color fundus photo and FFA of the left eye of the same patient. In addition to the features of acute stage of VKH, the macular area shows sub-retinal greenish-yellow lesion that demonstrates early minimal leakage on FFA and late staining suggestive of its predominant scar component. Right: Radial scan SS-OCT shows choroidal thickening (669 μm), blurred CSI, multiple neurosensory detachments with sub-retinal hyporeflective foci and hyperreflective amorphous deposits. Note the hyperreflective fusiform sub-foveal lesion. (D) Left: Radial scans SS-OCT during follow-up visits show resolution of the multifocal neurosensory detachment with persistence of the previously noted sub-retinal amorphous lesion. There is resolution of choroidal inflammation and improved visualization of the CSI. Bottom right: En-face SS-OCTA image and the corresponding flow-density map of the outer retina in a 6 × 6 mm field at 4-month follow-up visit show the hyperintense signal corresponding to high flow within neovascular complex. The abundant large mature vessels within the lesion denote a predominantly inactive CNV complex.

ellipsoid zone. SS-OCTA revealed loss of the normal hyperintense homogenous texture of the choriocapillaris and the development of moth-eaten like hypointense areas. SS-OCT examination of the left eye revealed large sub-foveal hyperreflective

lesion with complete disorganization of the outer retinal layers and minimal overlying subretinal fluid, reminiscent of inactive type 2 CNV. SS-OCTA examination of the left eye confirmed inactive CNV formation. After receiving systemic steroid treatment the patient had complete resolution of the acute attack, with restoration of the normal retinal architecture and normal choroidal thickness in the right eye. BCVA in the right eye improved to 6/6 (**Figure 1(A)–(D)**).

2.1.1.2 Case presentation

A 16-year-old female presenting with bilateral diminution of vision of approximately 2 weeks duration. Her BCVA was 6/60 bilaterally. Fundus examination of both eyes revealed multifocal serous retinal detachment in the posterior pole along with yellowish sub-retinal exudate formation and ONH hyperemia. FFA revealed numerous leaking points at the level of the RPE with pooling of dye into the sub-retinal space and hyperfluorescence of the ONH due to leakage from dilated optic disc vessels. Five months after the patient received high-dose steroid therapy, the fundus of both eyes showed resolution of the previously noted neurosensory detachments and development of diffuse RPE and choroidal pigmentary disturbances. The macular area of the left eye showed a sub-retinal greenish lesion suggestive of CNV formation.

2.1.1.2.1 SS-OCT and SS-OCTA features

The corresponding SS-OCT scan of the right eye in the chronic stage showed residual neurosensory detachment with persistent thickening of the choroid. SS-OCT of the left eye showed sub-retinal hyperreflective amorphous lesion corresponding to the macular lesion seen in the color photo. SS-OCT was inconclusive in differentiating the sub-retinal inflammatory material from CNV due to similar optical reflectance properties of both lesions. On the other hand, SS-OCTA of the left eye decisively excluded CNV formation (**Figure 2(A)** and **(B)**).

2.1.2 Serpiginous choroiditis

Serpiginous choroiditis is an autoimmune disorder characterized by primary choriocapillaropathy in the form of progressive vascular occlusion of the choriocapillaris and possibly larger choroidal vessels with secondary ischemic damage of the RPE and neurosensory retina. The classic presentation of the acute form is single or multiple sub-retinal creamy-white lesions developing at the edge of the optic disc and wind in the posterior pole in a centripetal serpentine or helical pattern. Less typical variants of the disease that do not have a peripapillary component include macular serpiginous, and ampiginous choroiditis. The latter form has an initial benign clinical presentation reminiscent of acute posterior multifocal placoid pigment epitheliopathy, and later follows a relentless progressive course. Serpiginous choroiditis is bilateral with propensity to recurrence. Disease re-activation is characterized by development of newer lesions at the edges of old healed scars. Chronic stage is characterized by diffuse atrophy and disappearance of the choriocapillaris with subsequent secondary atrophy of the RPE and outer retina, scarring and RPE pigmentary disturbances [33, 34]. The resultant choroidal thinning and loss of choriocapillaris will cause alteration of the normal structural OCT features in the form of forward bowing of the choroid with loss of the normal bowl-shaped configuration and anterior displacement of the Sattler's vessel layer, hence development of diffuse irregular flow-voids and enhanced visualization of the medium and large-sized choroidal vessels on OCTA slab of the choriocapillaris [35–37]. The disease

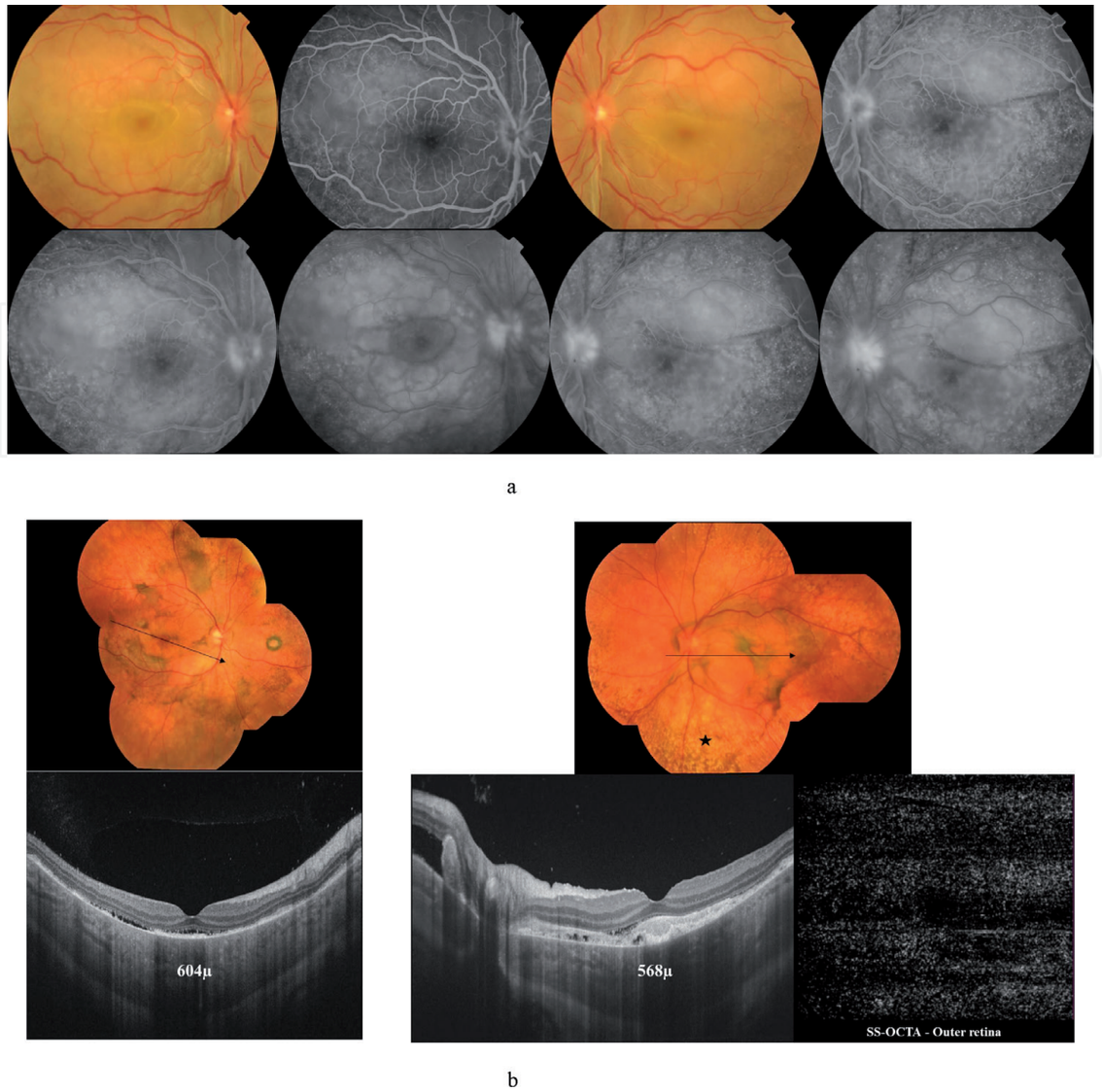

Figure 2.
(A) Color fundus photo and FFA of both eyes of a 16-year-old female with acute attack of VKH shows ONH hyperemia, and multiple neurosensory detachments with yellowish subretinal exudates. FFA demonstrates bilateral numerous leaking points at the level of the RPE. Note the classic starry-sky appearance that is characteristic of acute VKH. Later frames of FFA show pooling of dye into areas of multifocal neurosensory detachment, and ONH hyperfluorescence. (B) Top: Composite fundus photo of both eyes of the same patient 5 months later. The patient received high-dose systemic steroid treatment and developed chronic stage of VKH. Note the characteristic 'sunset glow' appearance of the fundus. Formation of Dalen-Fuchs nodules is more evident in the left eye (asterisk). Note the greenish sub-retinal lesion in the macular area in the left eye. Bottom left: High-definition line scan (12.0 mm) SS-OCT of the right eye shows irregular thickening of the RPE layer, sub-RPE and sub-retinal hyperreflective deposits, and residual neurosensory detachment. Note that the choroid is still grossly thickened. Bottom right: High-definition line scan (12.0 mm) SS-OCT of the left eye. Note the sub-foveal hyperreflective amorphous lesion corresponding to the macular lesion seen in the color photo. In this situation SS-OCT was inconclusive in excluding CNV formation. The corresponding en-face SS-OCTA image of the outer retina in a 6 × 6 mm field demonstrated normal hypointense appearance of an avascular outer retina, and decisively excluded CNV formation.

is notorious of aggressive course with propensity to involve the macular area and subsequent profound vision loss, which prompts briskly intervention with high-dose steroid therapy or other immunosuppressive agents for vision salvage [33].

2.1.2.1 Case presentation

A 28-year-old female patient who was a known case of bilateral serpiginous choroiditis. The patient presented with recent complaint of drop of vision approximately 1 month ago. Fundus examination in both eyes revealed large sharply circumscribed areas of sub-retinal fibrosis, with dense RPE clumps formation and

variable degree of RPE pigmentary disturbances. Some of the lesions have coalesced together forming a continuum of sub-retinal scarring that involved almost the entire posterior pole. The distribution of the lesions was suggestive of previous episodes of classic form of serpiginous choroiditis. BCVA was counting fingers (CF) at 50 cm and 3/60 in the right and left eyes, respectively.

2.1.2.1.1 SS-OCT and SS-OCTA features

SS-OCT in both eyes showed marked thinning of the choroid with loss of the normal bowl-shaped configuration due to severe erosion of the choriocapillaris. The outer retina showed marked disorganization and atrophy. The RPE-Bruch's complex, external limiting membrane layer (ELM) and inner segment-outer segment photoreceptors junction (IS/OS) were replaced by amorphous hyper-reflective material. SS-OCTA showed irregular hypointense areas of flow-void amidst areas of preserved choriocapillaris denoting patchy loss of choriocapillaris (**Figure 3(A)** and **(B)**).

2.1.2.2 Case presentation

A 37-year-old female patient who was a known case of bilateral serpiginous choroiditis presenting for routine follow-up. BCVA was 6/60 and 6/36 in the right and left eyes, respectively. The posterior pole in both eyes showed large well-circumscribed areas of extensive chorioretinal atrophy involving the peripapillary area and extending into the macular region. The retinal layers and even underlying choroidal vasculature have virtually disappeared from wide areas of the lesion with unveiling of the underlying sclera.

2.1.2.2.1 SS-OCT and SS-OCTA features

SS-OCT in both eyes showed marked thinning of the fovea, and marked disorganization and atrophy of the outer retinal layers. The choroid showed diffuse loss of the choriocapillaris and of the larger choroidal vessels with subsequent loss of the normal bowl-shaped configuration. SS-OCTA showed diffuse loss of the choriocapillaris with unveiling of the larger choroidal vessels (**Figure 4(A)** and **(B)**).

2.1.3 Multifocal choroiditis (MFC) and punctate inner choroidopathy (PIC)

MFC and PIC are idiopathic chorioretinal inflammatory disorders that are grouped under the spectrum of white dot syndromes. The phenotypic features of both entities overlap in many aspects to the extent that they are considered variants of the same disorder rather than separate clinical entities. MFC/PIC have predilection for young myopic females. Their hallmark is the development of yellowish-white chorioretinal lesions scattered throughout the posterior pole and the periphery of the fundus. Histologically, these lesions are composed of aggregates of inflammatory cells beneath the RPE that cause multifocal conical elevation of the RPE cell layer in the form of inflammatory PED. These lesions eventually break-through the RPE into the sub-retinal space with subsequent release of the inflammatory infiltrates into the outer retina. Recurrent episodes of inflammation cause structural retinal damage. The chorioretinal pathologic cascade is associated with vitritis that is most marked in cases of MFC compared to PIC. As chronicity ensues these lesions develop into punched-out chorioretinal scars [38–41]. Secondary CNV formation is a frequent complication, mounting up to one-third of cases, though some studies report much higher incidence [42–44]. CNV superimposed

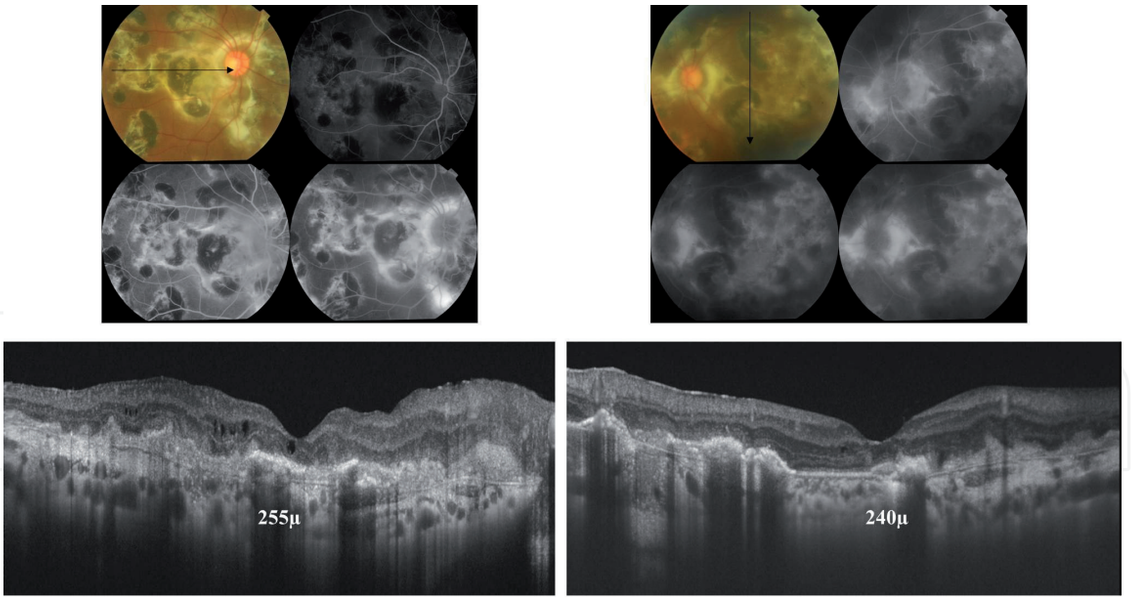

a

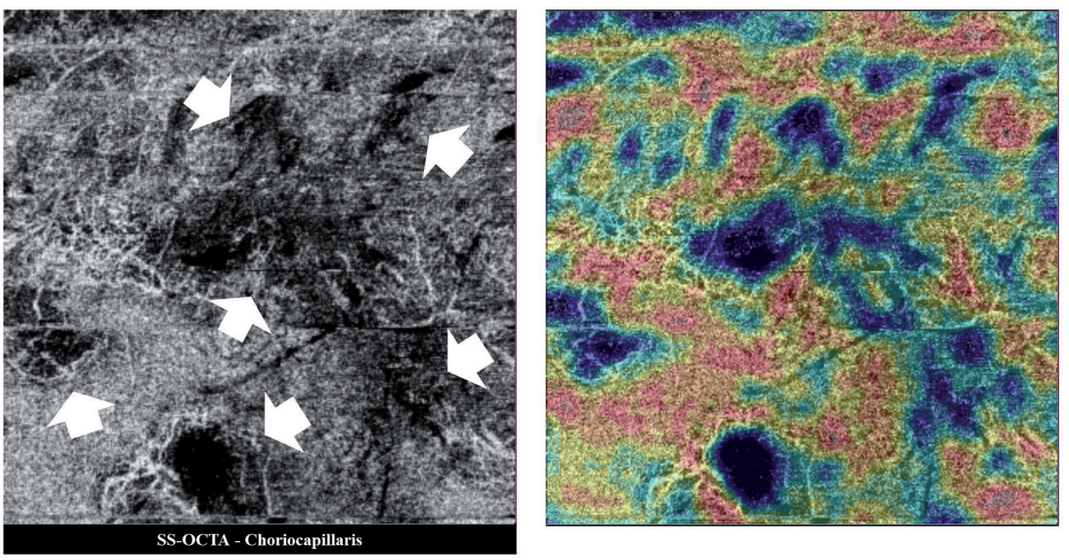

b

Figure 3.
(A) Top: Color fundus photo and FFA of both eyes of a 28-year-old female in chronic stage of serpiginous choroiditis. Note the diffuse plaques of sub-retinal fibrosis in the peripapillary area that radiate to involve almost the entire posterior pole. RPE pigment clumps formation is seen in the center of these lesions. On the corresponding FFA, these lesions show central blocked fluorescence surrounded by hyperfluorescent rim due to staining of the scar tissue. Bottom: Corresponding horizontal line scan (9.0 mm) SS-OCT (right), and vertical line scan (9.0 mm) SS-OCT (left) of both eyes show marked thinning of the choroid (255 and 240 µm in the right and left eyes, respectively). Note the irregular choroidal contour, marked thinning of the choriocapillaris and enhanced visualization of larger-sized choroidal vessels. The RPE-Bruch's complex, ellipsoid zone, ELM and IS/OS could not be identified and are replaced by amorphous hyper-reflective deposits. Note the foveal thinning and marked disorganization of the overlying neurosensory retina. (B) En-face SS-OCTA image and the corresponding flow density map of the choriocapillaris of the right eye in a 3 × 3 mm field. There are scattered sharply circumscribed areas of flow-voids due to loss of choriocapillaris (white arrows) with corresponding blue shades on the flow-density map. Note the enhanced visualization of the hyperintense signal of the larger choroidal vessels at the edges of the flow-voids and elsewhere due to combination of compensatory dilatation and anterior displacement of Sattler's vessel layer.

on MFC/PIC is usually a type 2 variant and is notoriously difficult to detect or to follow-up its response to anti-vascular endothelial growth factor (anti-VEGF) agents using conventional angiography techniques or structural OCT because it is characterized by minimal leakage on angiography and fluid accumulation on OCT, in addition to overlapping angiographic and OCT features with MFC/PIC-induced inflammation [10].

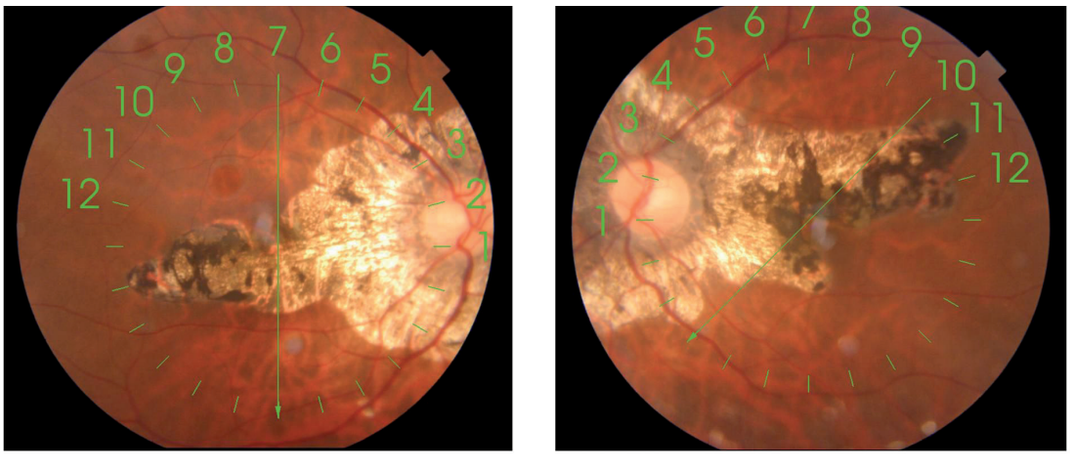

a

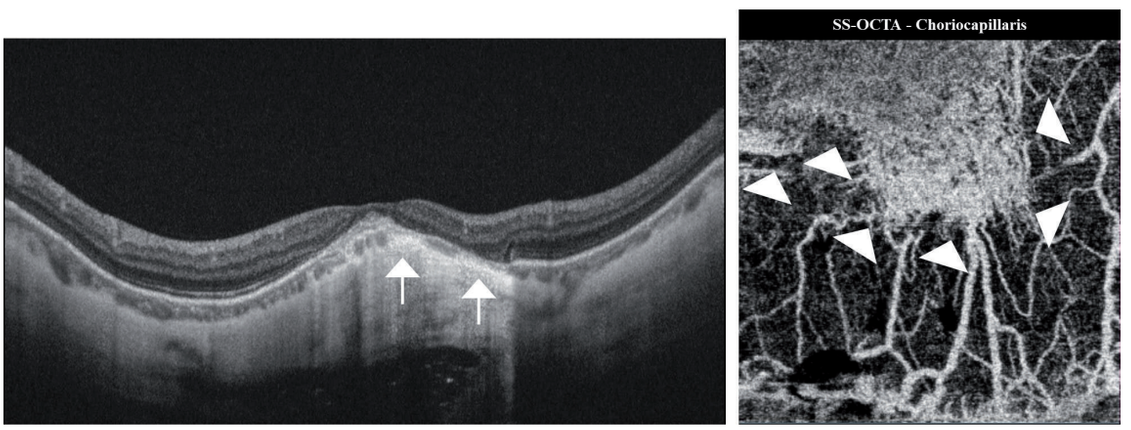

b

Figure 4.
(A) Color fundus photo of both eyes of a 37-year-old female with advanced posterior pole scarring secondary to serpiginous choroiditis. The retinal layers and underlying choroidal vasculature have virtually disappeared from the peripapillary and macular areas with secondary RPE pigment clumps formation. (B) Left: Radial scan SS-OCT of the right eye. Note almost complete disappearance of the choriocapillaris. The larger-sized choroidal vessel layer is thinned and has even disappeared in some areas (white arrows). In the sub-foveal area, a combination of severe atrophy of the neurosensory retina, RPE, choriocapillaris and marked anterior bowing of the choroid has resulted in enhanced optical reflectance of the choroid and underlying sclera. Right: Corresponding en-face SS-OCTA image at the level of the choriocapillaris in a 3 × 3 mm field. The choriocapillaris has been reduced to a small patch (white arrowheads) with near complete wiping of remaining parts and readily visualization of the larger choroidal vessels.

2.1.3.1 Case presentation

A 37-year-old female who is a known case of PIC presenting with drop of vision in the right eye of approximately 2-month duration. BCVA was 5/60 and 6/12 in the right and left eyes, respectively. Fundus examination of the right eye revealed features of myopic fundus with multiple discrete punched-out sub-retinal lesions scattered in the posterior pole and extending towards the equator. Most lesions were yellowish-white in color, whereas few lesions demonstrated variable degree of pigmentation. The foveal area showed a grayish sub-retinal lesion that exhibited typical features of classic CNV on FFA. SS-OCT confirmed the presence of type 2 CNV. SS-OCTA demonstrated hyperintense signal and characteristic features of active CNV. The patient received anti-VEGF injections for the right eye. At this stage her left fundus showed tessellated appearance with peripapillary atrophy due to myopia without signs of PIC. The patient returned 9 months later with complaints of metamorphopsia in the left eye. BCVA in the left eye has dropped to 6/18. Fundus examination revealed multiple scattered sub-retinal creamy white lesions. She was started on oral steroid therapy and the fundus

lesions went onto remission though metamorphopsia persisted. Three months later she presented with worsening metamorphopsia and more drop of vision. BCVA in the left eye was 6/36. FFA, SS-OCT, and SS-OCTA revealed presence of CNV.

2.1.3.1.1 SS-OCT and SS-OCTA features

SS-OCT showed sub-RPE hyperreflective knob-like projections either confined to the sub-RPE space or breaking through into the sub-retinal space. SS-OCTA of the choriocapillaris revealed scattered foci of flow-voids corresponding to the location of the scarred punched-out lesions in the fundus. The foveal lesion suggestive of neovascular growth on color fundus photo and on FFA appeared as a sub-foveal amorphous hyperreflective material above the RPE suggestive of type 2 CNV with minimal overlying fluid. SS-OCTA at the level of the outer retina confirmed the hyperintense signal of flow within neovascular complex (**Figures 5(A)** and **(B)** and **6(A)** and **(B)**).

2.1.3.2 Case presentation

A 31-year-old female who is a known case of MFC presented with drop of vision in the left eye of approximately 3 weeks duration. BCVA was 6/6 and 3/60 in the right and left eyes, respectively. Fundus examination in the left eye revealed a sub-foveal yellowish-white lesion approximately 1 disc diameter (DD) in size. The posterior pole temporal to the lesion showed sub-retinal punched-out healed lesions of old episode of MFC. FFA demonstrated sub-foveal classic CNV formation. SS-OCT and SS-OCTA confirmed presence of neovascular growth. The patient started anti-VEGF injection that caused regression of the CNV. Her BCVA in the left eye after 3 ranibizumab injections and 7-month follow-up was 6/24.

2.1.3.2.1 SS-OCT and SS-OCTA features

SS-OCT examination revealed the presence of type 2 CNV with minimal overlying sub-retinal fluid. SS-OCTA revealed the hyperintense signal characteristic of flow within active neovascular network. On follow-up visits after the patient received anti-VEGF intravitreal injections, the morphology of the CNV on SS-OCT showed minimal variation. On the other hand, SS-OCTA was conclusive in documenting the regression of the CNV in response to anti-VEGF treatment (**Figure 7(A)** and **(B)**).

2.2 Infectious uveitides

2.2.1 Toxoplasmosis

Ocular toxoplasmosis is an infectious granulomatous posterior uveitis. The disease is considered the most common cause of posterior uveitis worldwide. Ocular involvement occurs as part of systemic toxoplasmosis. Infection is either congenital via transplacental transmission of the protozoan *Toxoplasma gondii* form an infected mother, or acquired due to ingestion of contaminated water or food or ingestion of undercooked meat containing toxoplasma cysts [45]. The clinical presentation is in the form of focal necrotizing retinochoroiditis in the posterior pole. The lesion can develop de novo or can present in the form of a satellite lesion, which is an acute focus of retinochoroiditis developing adjacent to an old chorioretinal scar. The lesion is associated with overlying vitritis which could be severe enough to obscure visualization of the fundus apart from the yellowish-white necrotizing focal lesion giving rise to the characteristic spotlight-in-the-fog appearance. As the acute episode subsides, a quiescent hyperpigmented scar

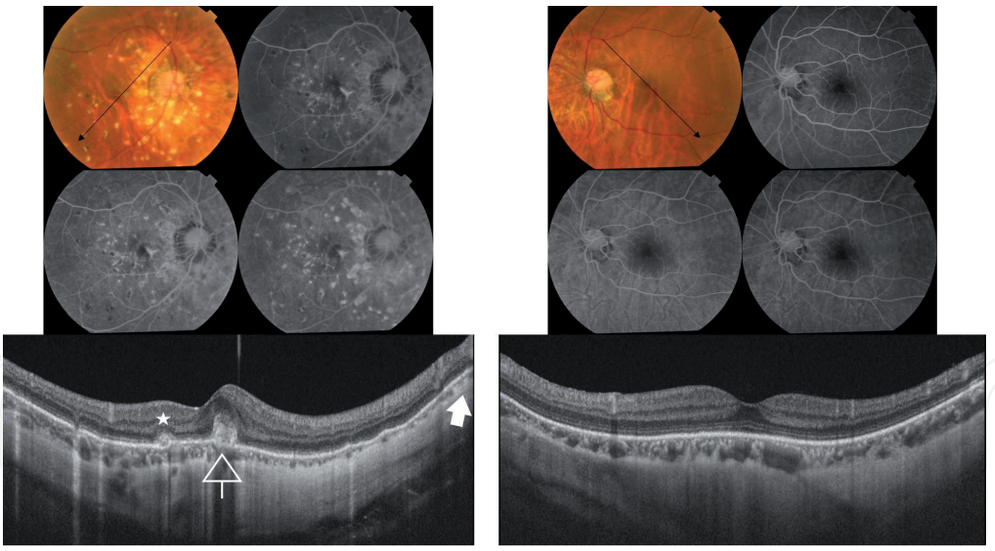

a

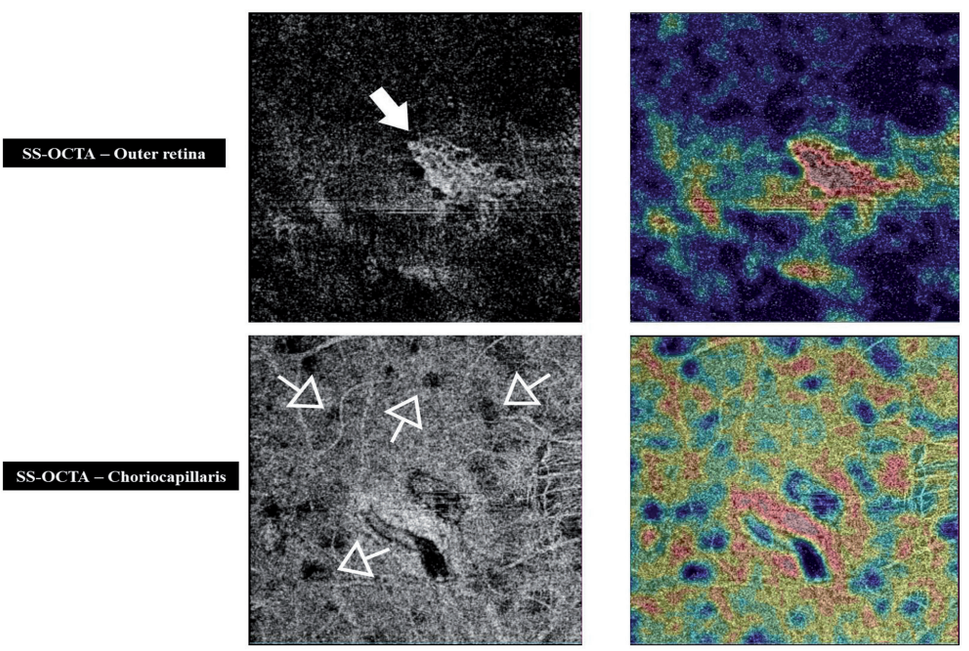

b

Figure 5.
(A) Top: Color fundus photo and FFA of the right and left eyes, respectively of a 37-year-old female with PIC. The right fundus shows multiple yellowish-white punched-out lesions scattered in the posterior pole and extending towards the equator. Some of these lesions show RPE clump deposition. The foveal area shows a sub-retinal grayish lesion. The fundus shows features of myopia as tessellated appearance and peripapillary chorioretinal atrophy. On FFA, the punched-out lesions seen in the color photo demonstrate early hyperfluorescence that gradually increases in intensity throughout successive frames due to combined pooling in PED and late staining. The lesions maintain sharply circumscribed boundaries without leakage of dye. Some of these lesions show blocked fluorescence due to masking by RPE clump formation. The foveal lesion shows early hyperfluorescence that gradually increases in intensity throughout successive frames due to minimal leakage. Color fundus photo and FFA of the left eye show myopic features. Bottom left: Radial scan SS-OCT of the right eye shows knob-like projections in the sub-RPE space (white arrow). One of these projections broke through into the sub-retinal space (asterisk). Note the sub-foveal hyperreflective amorphous lesion with minimal overlying fluid, suggestive of type 2 CNV formation (open arrow). Bottom right: Radial scan SS-OCT of the left eye showed choroidal thinning due to myopia. (B) Top: En-face SS-OCTA image in a 3 × 3 mm field at the level of the outer retina and the corresponding flow-density map show the hyperintense signal characteristic of flow within neovascular tissue (white arrow). The CNV shows dense arborization and anastomosis, which are characteristic of activity. Bottom: En-face SS-OCTA image in a 6 × 6 mm field at the level of the choriocapillaris and the corresponding flow-density map show the moth-eaten appearance of the choriocapillaris due to presence of scattered flow-voids (white open arrows) denoting foci of vascular atrophy and that correspond to the location of the punched-out lesions seen in the color photo.

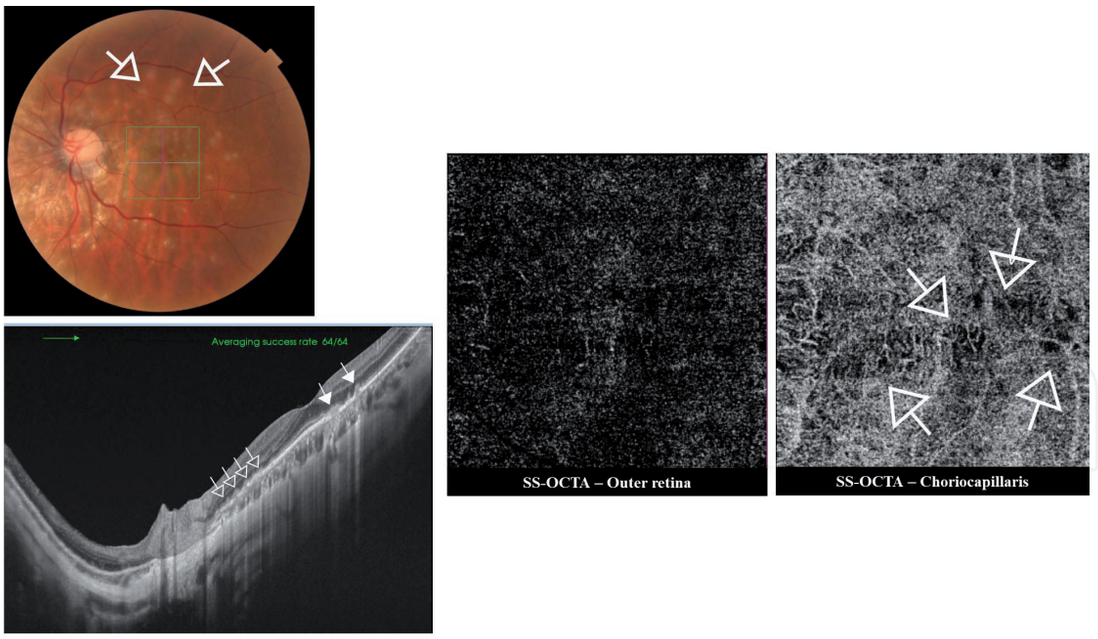

a

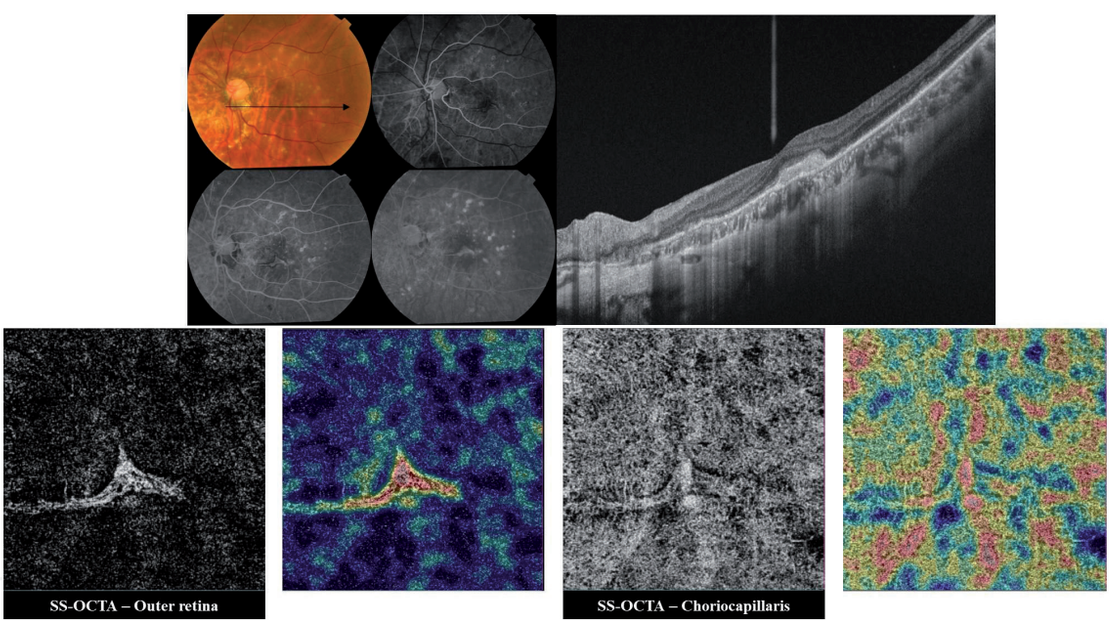

b

Figure 6.
(A) Top left: Color photo of the left fundus of the same patient in ***Figure 5****. Note the multiple creamy white lesions that developed in the posterior pole. Note the indistinct boundaries of some of these lesions (white open arrows), which indicate their recent onset compared to the atrophic punched-out appearance of the older lesions seen in the right fundus. Right: En-face SS-OCTA images in a 3 × 3 mm field of the outer retina and of the choriocapillaris. Note the normal appearance of the avascular outer retina, and the development of multiple foci of flow-voids in the choriocapillaris corresponding to the sub-retinal lesions seen in color photo. Bottom left: High-definition line scan (12.0 mm) SS-OCT of the left eye. Note the newly developed hyperreflective knob-like projections of the RPE cell layer (white open arrows). Some of these projections broke through the RPE into the sub-retinal space (white closed arrows). (B) Top left: Color fundus photo and FFA of the same patient 3 months later. Note the newly developed neovascular membrane in the foveal area. Top right: Radial scan SS-OCT shows newly developed sub-foveal hyperreflective amorphous lesion above the RPE, suggestive of type 2 CNV formation. Bottom left: En-face SS-OCTA image and the corresponding flow-density map of the outer retina in a 3 × 3 mm field show the hyperintense signal of the newly developed CNV. The dense arborization and anastomosis within the lesion are indicators of activity. Bottom right: En-face SS-OCTA image and the corresponding flow-density map of the choriocapillaris in a 3 × 3 mm field show multifocal hypointense signal due to flow-voids, which could result from multifocal atrophy of choriocapillaris due to older lesions or from signal masking in newer ones.*

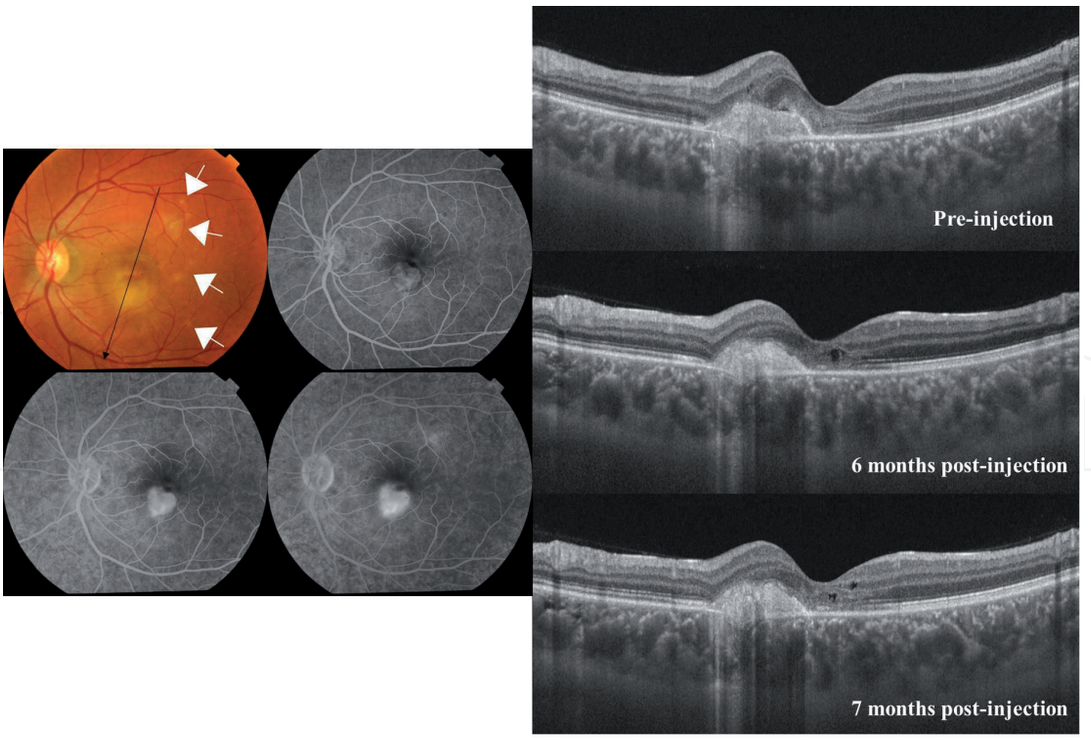

A

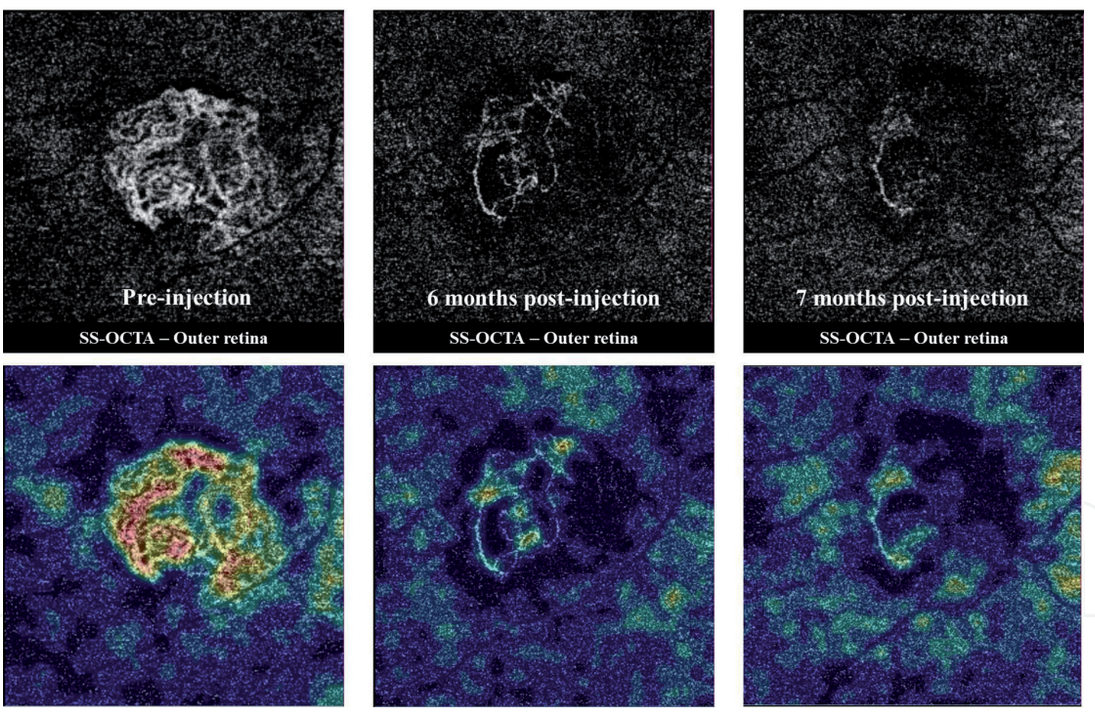

B

Figure 7.
(A) Left: Color fundus photo and FFA of the left eye of a 31-year-old female with MFC complicated by CNV formation. The fundus shows a sub-foveal yellowish-white lesion approximately 1 DD in size. Note the multiple whitish punched-out lesions located temporally and denote healed MFC lesions (white arrows). On FFA, the sub-foveal lesion demonstrates early well-circumscribed hyperfluorescence with late profuse leakage beyond the boundaries of the lesion. Right: Radial scan mode SS-OCT shows hyperreflective amorphous lesion lying entirely above the RPE with minimal overlying hyporeflective sub-retinal fluid. Note the minimal variation in the lesion morphology in follow-up SS-OCT scans, hence inconclusive information on CNV response to therapy. (B) En-face SS-OCTA images of the outer retina and the corresponding flow-density maps in a 3 × 3 mm field at initial presentation (left) and during follow-up visits after receiving anti-VEGF treatment (middle and right). At presentation, SS-OCTA of the outer retina demonstrated the hyperintense signal characteristic of flow within neovascular growth. Note the extensive anastomosis and dense arborization within the lesion, which indicate active CNV. Note the unequivocal SS-OCTA depiction of gradual regression of the CNV lesion during follow-up visits in response to anti-VEGF treatment.

develops which could lead to profound visual loss should it affect the macula or the papillomacular bundle [18]. On structural OCT, an active lesion features thickening and disorganization of the neurosensory retina, thickening of the choroid underlying the lesion and evidence of vitritis in the form of hyperreflective dots and thickening of the posterior hyaloid. As the lesion heals, the patient develops a chorioretinal scar with marked thinning and disorganization of the neurosensory retina and thinning of the underlying choroid. Choroidal neovascularization and vitreoretinal interface disturbances in the form of vitreoretinal tractional bands can develop [17, 18, 46].

2.2.1.1 Case presentation

A 13-year-old male presented to our clinic complaining of diminution of vision in his right eye of 3 days duration. Fundus examination revealed whitish retinal lesion inferonasal to the ONH with feathery indistinct edges and overlying vitritis. The ONH was inflamed with blurred edges. BCVA was 6/60 and 6/6 in the right and left eyes, respectively. Due to proximity of the lesion to the optic disc and the macula, we started the patient on oral sulfadiazine, pyrimethamine, and folinic acid. Oral steroids were started 24 h after initiation of antimicrobial regimen. At 2-month follow-up visit, the fundus showed resolution of previously noted vitritis and disc hyperemia, and regression of the retinal lesion, which appeared smaller in size and had well-defined boundaries. BCVA in the right eye improved to 6/6.

2.2.1.1.1 SS-OCT and SS-OCTA features

SS-OCT showed focal thickening with complete disorganization of the neurosensory retina, disruption of the ELM, IS/OS, and RPE cell layer with focal thickening of the choroid beneath the lesion. The overlying vitreous showed dense infiltration with hyperreflective foci indicating vitritis. SS-OCTA showed localized hypointense signal in the SCP, DCP, and choriocapillaris corresponding due to the masking by the focal lesion. During follow-up the previously noted hypointense signal regressed in size in proportion to regression of the lesion (**Figure 8(A)** and **(B)**).

2.2.1.2 Case presentation

A 26-year-old female presented to our clinic complaining of diminution of vision in her right eye of 1 week duration. Fundus examination revealed yellowish-white retinal lesion composed of a larger focus and smaller adjacent lesions overlying the papillomacular bundle. BCVA was 6/24 and 6/6 in the right and left eyes, respectively. As the lesion involved the papillomacular bundle, the patient was started on oral sulfadiazine, pyrimethamine, and folinic acid. Oral steroids were started 24 h after initiation of antimicrobial regimen.

2.2.1.2.1 SS-OCT and SS-OCTA features

SS-OCT showed focal thickening with complete disorganization of the neurosensory retina, disruption of the ELM, IS/OS, and RPE cell layer with focal thickening of the choroid beneath the lesion. The posterior hyaloid was thickened and partially attached to the focal retinal lesion. SS-OCTA showed localized hypointense signal in the SCP, DCP, and choriocapillaris corresponding to the masking effect of the focal lesion (**Figure 9(A)** and **(B)**).

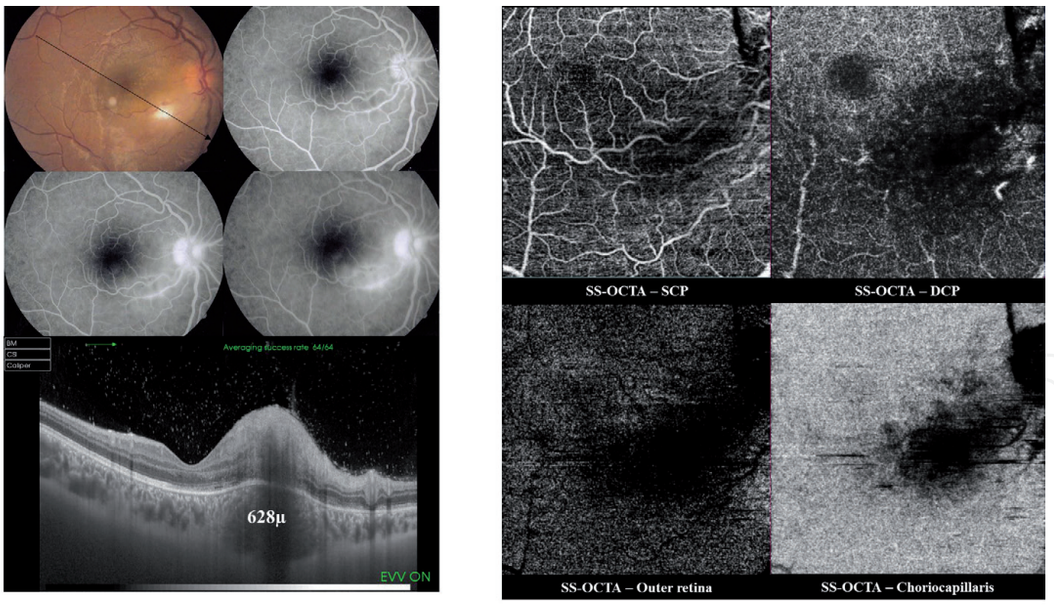

a

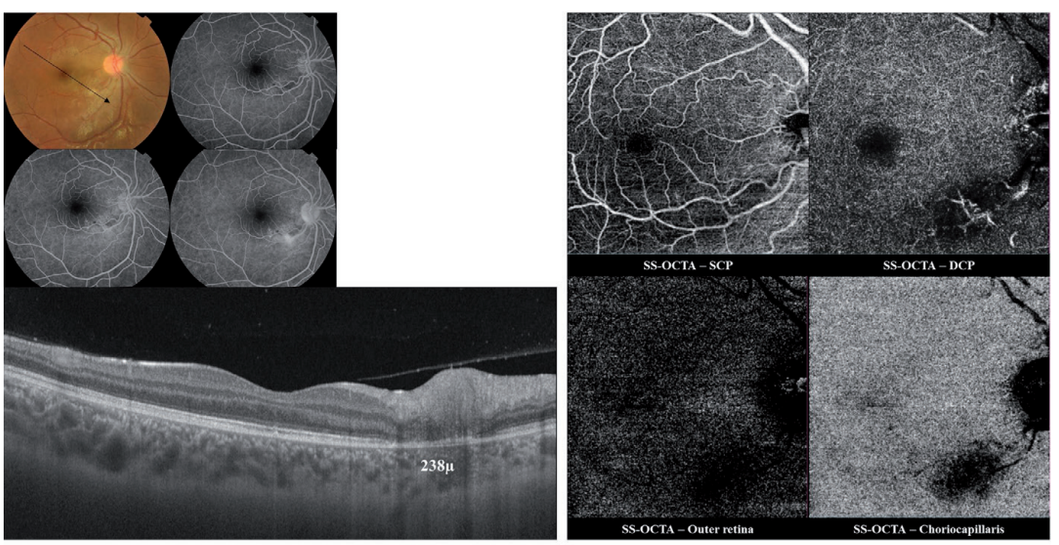

b

Figure 8.
(A) Top left: Color fundus photo and FFA of the right eye of a 13-year-old male with acute toxoplasma retinochoroiditis. The fundus shows a whitish retinal lesion inferotemporal to ONH with blurred edges and overlying vitritis. The ONH shows hyperemia and engorged peripapillary vessels. The corresponding FFA shows early localized blocked fluorescence corresponding in size and location to the lesion seen in color photo. Later frames show leakage from adjacent focal retinal vasculitis. The ONH demonstrates hyperfluorescence due to leakage form inflamed optic disc vessels. Bottom left: High-definition line scan (12.0 mm) SS-OCT shows focal thickening of the retina temporal to the optic disc with marked disorganization of the retinal layers and increased optical reflectance giving the affected part a blurred hyperreflective appearance known as the smudge effect, and causing optical shadowing of the underlying choroid. Note focal disruption of the ELM, and IS/OS layers in the area of the lesion. The choroid underlying the focal lesion is markedly thickened (628 µm), with focal blurring of the CSI. The overlying vitreous shows dense infiltration with hyperreflective foci, which represent inflammatory cell infiltrates. Right: En-face SS-OCTA images in a 6 × 6 mm field of the SCP, DCP, outer retina, and the choriocapillaris show hypointense signal caused by masking of the vascular layers and overshadowing of the outer retina by the focal lesion and overlying vitreous opacity. (B) Top left: Color fundus photo and FFA of the right eye at 2-month follow-up visit. Note resolution of vitritis, optic disc swelling, and a smaller size well-defined residual lesion. The corresponding FFA shows significantly improved retinal vasculitis and minimal leakage from the optic disc vessels. Bottom left: Radial scan SS-OCT shows complete resolution of choroidal inflammation (choroidal thickening measured 238 µm), with a well-defined CSI. The previously noted hyperreflective foci in the vitreous disappeared almost completely. There is significant improvement in the previously noted focal thickening of the retina, though with persistent disorganization of retinal layers and disruption of ELM and IS/OS layers. Top right: En-face SS-OCTA images of the SCP, DCP, outer retina, and the choriocapillaris in a 6 × 6 mm field show marked regression of the previously noted hypointense signal and improved visualization of the normal architecture of the vascular layers and of the outer retina.

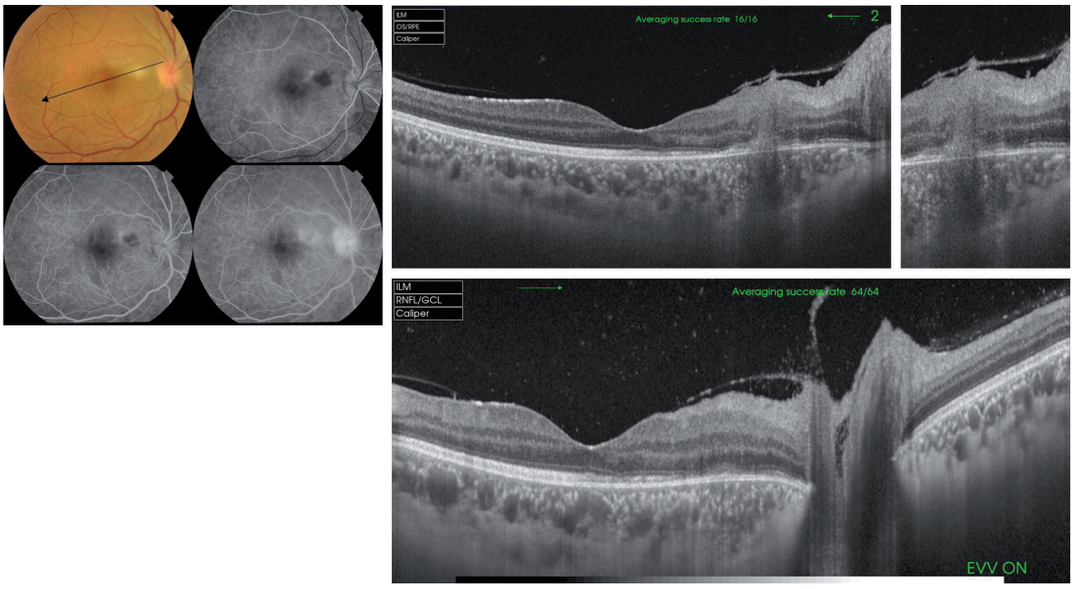

a

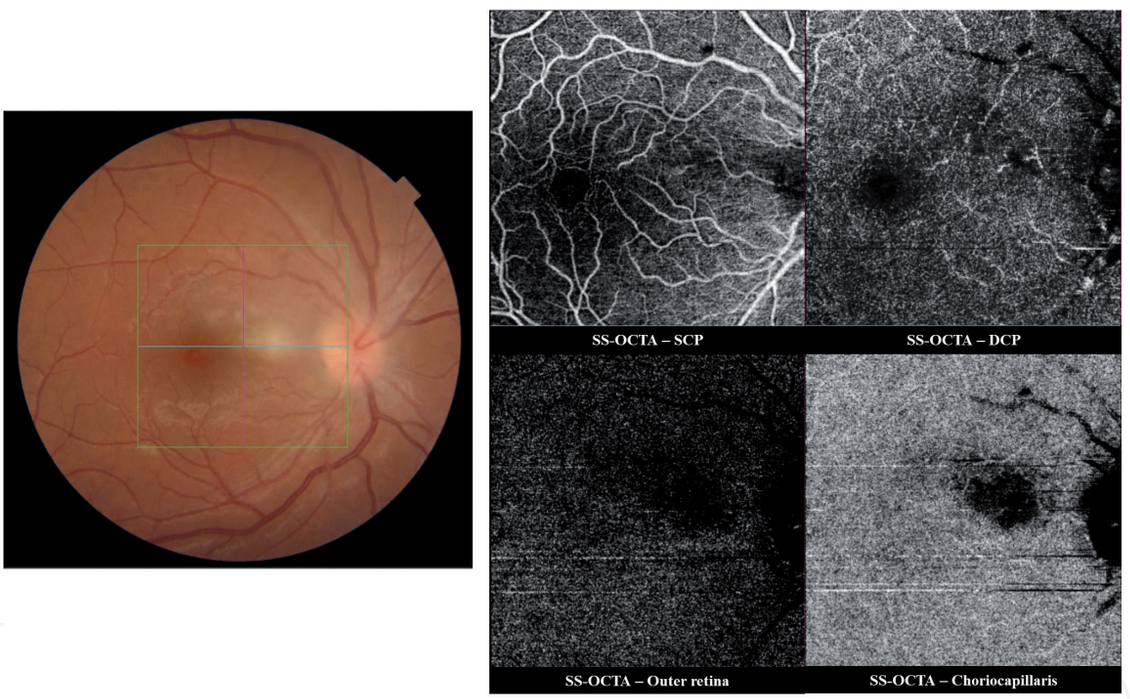

b

Figure 9.
(A) Top left: Color fundus photo and FFA of the right eye of a 26-year-old female with acute toxoplasma retinochoroiditis. Note the yellowish-white lesions overlying the papillomacular bundle that consist of a single larger focus and adjacent smaller ones. The partially blurred appearance of the optic disc and the papillomacular bundle is caused by vitritis overlying the lesion. FFA shows localized blocked fluorescence corresponding in size and location to the lesion seen in color photo. In later frames, leakage from adjacent focal retinal vasculitis causes hyperfluorescence. The ONH demonstrates hyperfluorescence due to leakage from inflamed disc vessels. Top middle: Radial scan SS-OCT shows focal thickening of the retina temporal to the optic disc with marked disorganization of the retinal layers and increased optical reflectance giving the affected part a blurred hyperreflective appearance known as the smudge effect, and causing optical shadowing of the underlying choroid. The ELM, IS/OS layers are disrupted. The choroid underlying the focal lesion is thickened. The overlying vitreous shows thickening of the posterior hyaloid which is partially attached to the focal retinal lesion. Top right: A zoom-in on the attachment between the focal retinal lesion and the posterior hyaloid. Bottom: High-definition line scan (12.0 mm) SS-OCT with the enhanced vitreous visualization (EVV) mode turned-on. Note the multiple hyperreflective dots scattered in the vitreous cavity and deposited along the posterior hyaloid face. (B) En-face SS-OCTA images of the SCP, DCP, outer retina and the choriocapillaris in a 6 × 6 mm field show hypointense signal caused by masking of the vascular layers and overshadowing of the outer retina by the focal lesion.

2.2.1.3 Case presentation

A female child, 8 years old presented to our office. Her mother reported noticing deviation of the right eye of her child and poor vision upon covering the left eye. BCVA was HM and 6/6 in the right and left eyes, respectively. Fundus examination of the right eye revealed a large saucer-shaped deeply excavated pigmented chorio-retinal scar occupying the macular area.

2.2.1.3.1 SS-OCT and SS-OCTA features

SS-OCT showed marked thinning and disorganization of the retina, irregular elevation and thickening of the RPE and altered choroidal contour. SS-OCTA showed complete loss of the choriocapillaris at the site of the scar with unveiling of the large choroidal vessels underneath (**Figure 10**).

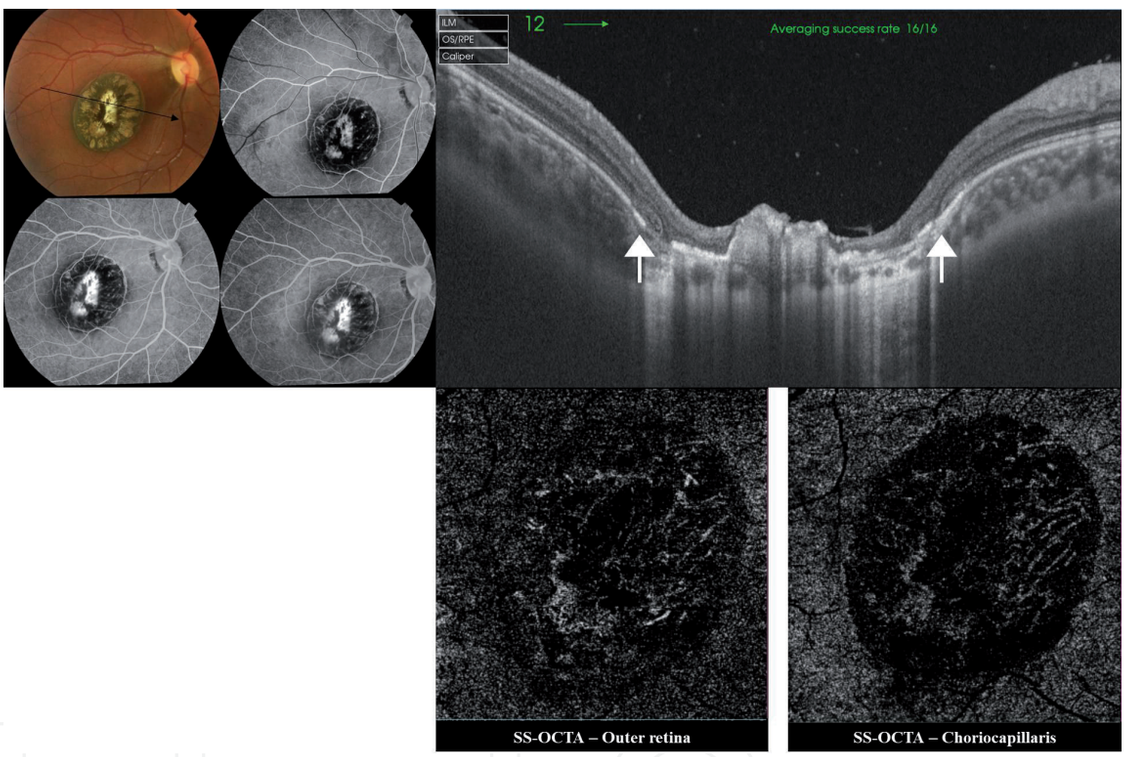

Figure 10.
Top left: Color fundus photo and FFA of the right eye of an 8-year-old female child with old toxoplasmosis scar. The macular area is almost entirely occupied by a large oval chorioretinal scar with sharply-circumscribed edges. The lesion shows variable grades of RPE pigmentary disturbances. The central part of the lesion shows complete chorioretinal atrophy exposing the underlying sclera. Note that the scar is sharply focused in comparison to the slightly defocused ONH and peripapillary area, which indicates the deeper plane of the scar due to excavation. On FFA, the lesion shows alternating areas of blocked fluorescence due to RPE pigment clumps formation and hyperfluorescence due to staining of scar tissue. Top right: Radial scan SS-OCT of the macular area. Note the abrupt transition from normal retinal layers at the edges of the lesion (white arrows) to marked thinning and disorganization of the neurosensory retina in the scar area. The central part of the lesion shows lumpy hyperreflective amorphous lesion representing the thickened distorted RPE layer. The underlying choroid is markedly thinned with increased optical reflectivity due to enhanced light penetration through the over-thinned layers. Bottom: En-face SS-OCTA images of the outer retina and choriocapillaris. The overthinning of the retina, and loss of choriocapillaris at the site of chorioretinal scar led to enhanced visualization of the Sattler's layer in the choriocapillaris and outer retina slabs.

3. Conclusion

The introduction of SS-OCT and SS-OCTA technology greatly propelled the management course of uveitis by unveiling previously unexplored areas of retinal and choroidal pathological morphology in uveitides, and by introducing new

inflammatory biomarkers that helped monitoring the disease response to various therapeutic agents. The non-invasive nature of the new technology added to its versatility in particular clinical situations in which conventional angiography could be impractical or hazardous especially in lengthy follow-up protocols, pediatric patients, pregnant females, and patients with severely compromised renal function. However, this nascent technology should be considered an important complimentary tool to conventional angiographic tests without substituting them. Conventional FFA and ICG still maintain the lead role in diagnosis of uveitides by providing yet unmatched information on *leakage* which is by far the most important biomarker in monitoring the state of inner blood-retina-barrier in inflammatory entities as uveitides.

Author details

Magdy Moussa[1,2*] and Mahmoud Leila[3]

1 Ophthalmology, Ophthalmology Department, Faculty of Medicine, Tanta University, Tanta, Egypt

2 MEDIC Eye Center, Tanta, Egypt

3 Ophthalmology, Retina Department, Research Institute of Ophthalmology, Giza, Egypt

*Address all correspondence to: magdymoussa60@gmail.com

References

[1] Richard G, Soubrane G, Yannuzzi LA. The principles of fluorescein angiography. In: Fluorescein and ICG Angiography. Textbook and Atlas. 2nd ed. New York: Thieme; 1998. pp. 66-101

[2] Staurenghi G, Bottoni F, Giani A. Clinical applications of diagnostic indocyanine green angiography. In: Ryan SJ, editor. Retina. 6th ed. Philadelphia: Saunders; 2018. pp. 46-76

[3] Pichi F, Sarraf D, Morara M, Mazumdar S, Neri P, Gupta V. Pearls and pitfalls of optical coherence tomography angiography in the multimodal evaluation of uveitis. Journal of Ophthalmic Inflammation and Infection. 2017;**7**:20. DOI: 10.1186/s12348-017-0138-z

[4] Agarwal A, Invernizzi A, Singh RB, Foulsham W, Aggarwal K, Handa S, et al. An update on inflammatory choroidal neovascularization: Epidemiology, multimodal imaging, and management. Journal of Ophthalmic Inflammation and Infection. 2018;**8**:13. DOI: 10.1186/s12348-018-0155-6

[5] Bonnin S, Mané V, Couturier A, et al. New insight into the macular deep vascular plexus imaged by optical coherence tomography angiography. Retina. 2015;**35**:2347-2352

[6] Coscas F, Glacet-Bernard A, Miere A, et al. Optical coherence tomography angiography in retinal vein occlusion: Evaluation of superficial and deep capillary plexa. American Journal of Ophthalmology. 2016;**161**:160-171

[7] Spaide RF, Klancnik JM Jr, Cooney MJ. Retinal vascular layers imaged by fluorescein angiography and optical coherence tomography angiography. JAMA Ophthalmology. 2015;**133**(1):45-50

[8] De Carlo TE, Romano A, Waheed NK, et al. A review of optical coherence tomography angiography (OCTA). International Journal of Retina and Vitreous. 2015;**1**:5

[9] Wang Q, Chan S, Yang JY, et al. Vascular density in retina and choriocapillaris as measured by optical coherence tomography angiography. American Journal of Ophthalmology. 2016;**168**:95-109

[10] Levison AL, Baynes KM, Lowder CY, Kaiser PK, Srivastava SK. Choroidal neovascularisation on optical coherence tomography angiography in punctate inner choroidopathy and multifocal choroiditis. The British Journal of Ophthalmology. 2017;**101**(5):616-622

[11] Grulkowski I, Liu JJ, Potsaid B, Jayaraman V, Lu CD, Jiang J, et al. Retinal, anterior segment and full eye imaging using ultrahigh speed swept source OCT with vertical-cavity surface emitting lasers. Biomedical Optics Express. 2012;**3**(11):2733-2751

[12] Stanga PE, Tsamis E, Papayannis A, Stringa F, Cole T, Jalil A. Swept-source optical coherence tomography angiography ™ (Topcon Corp, Japan): Technology review. Developments in Ophthalmology. 2016;**56**:13-17

[13] Ikuno Y, Maruko I, Yasuno Y, Miura M, Sekiryu T, Nishida K, et al. Reproducibility of retinal and choroidal thickness measurements in enhanced depth imaging and high-penetration optical coherence tomography. Investigative Ophthalmology & Visual Science. 2011;**52**:5536-5540

[14] Fong AHC, Li KKW, Wong D. Choroidal evaluation using enhanced depth imaging spectral-domain optical coherence tomography in Vogt-Koyanagi-Harada disease. Retina. 2011;**31**:502-509

[15] Maruko I, Iida T, Sugano Y, Oyamada H, Sekiryu T, Fujiwara T, et al. Subfoveal choroidal thickness after treatment of Vogt-Koyanagi-Harada disease. Retina. 2011;**31**:510-517

[16] Nakayama M, Keino H, Okada AA, Watanabe T, Taki W, Inoue M, et al. Enhanced depth imaging optical coherence tomography of the choroid in Vogt-Koyanagi-Harada disease. Retina. 2012;**32**:2061-2069

[17] Chen KC, Jung JJ, Engelbert M. Single acquisition of the vitreous, retina and choroid with swept-source optical coherence tomography in acute toxoplasmosis. Retinal Cases & Brief Reports. 2016;**10**:217-220

[18] Goldenberg D, Goldstein M, Loewenstein A, Habot-Wilner Z. Vitreal, retinal and choroidal findings in active and scarred toxoplasmosis lesions: A prospective study by spectral-domain optical coherence tomography. Graefe's Archive for Clinical and Experimental Ophthalmology. 2013;**251**:2037-2045

[19] Gao SS, Liu G, Huang D, Jia Y. Optimization of the split-spectrum amplitude-decorrelation angiography algorithm on a spectral optical coherence tomography system. Optics Letters. 2015;**40**(10):2305-2308

[20] Kuehlewein L, Tepelus TC, An L, Durbin MK, Srinivas S, Sadda SR. Noninvasive visualization and analysis of the human parafoveal capillary network using swept source OCT optical microangiography. Investigative Ophthalmology & Visual Science. 2015;**56**(6):3984-3988

[21] Savastano MC, Lumbroso B, Rispoli M. In vivo characterization of retinal vascularization morphology using optical coherence tomography angiography. Retina. 2015;**35**(11):2196-2203

[22] Spaide RF. Volume-rendered angiographic and structural optical coherence tomography. Retina. 2015;**35**:2181-2187

[23] Astroz P, Miere A, Mrejen S, Sekfali R, Souied EH, Jung C, et al. Optical coherence tomography angiography to distinguish choroidal neovascularization form macular inflammatory lesions in multifocal choroiditis. Retina. 2018;**38**:299-309

[24] Nakao S, Kaizu Y, Oshima Y, Sakamoto T, Ishibashi T, Sonoda KH. Optical coherence tomography angiography for detecting choroidal neovascularization secondary to punctate inner choroidopathy. Ophthalmic Surgery, Lasers and Imaging Retina. 2016;**47**(12):1157-1161

[25] Kotsolis AI, Killian FA, Ladas ID, Yannuzzi LA. Fluorescein angiography and optical coherence tomography concordance for choroidal neovascularization in multifocal choroiditis. The British Journal of Ophthalmology. 2010;**94**:1506-1508

[26] Vance SK, Khan S, Klancnik JM, Freund KB. Characteristics of spectral-domain optical coherence tomography findings of multifocal choroiditis. Retina. 2011;**31**:717-723

[27] Nussenblatt RB. Vogt-Koyanagi-Harada syndrome. In: Nussenblatt RB, Whitcup SM, editors. Uveitis. Fundamentals and Clinical Practice. 4th ed. Vol. 2010. USA: Mosby. pp. 303-318

[28] Goto H, Rao PK, Rao NA. Vogt-Koyanagi-Harada disease. In: Ryan SJ, editor. Retina. 6th ed. Philadelphia: Saunders; 2018. pp. 1505-1515

[29] Baltmr A, Lightman S, Tomkins-Netzer O. Vogt-Koyanagi-Harada syndrome—Current perspectives. Clinical Ophthalmology. 2016;**10**:2345-2361

[30] Rao NA. Pathology of Vogt-Koyanagi-Harada disease. International Ophthalmology. 2007;**27**:81-85

[31] Aggarwal K, Agarwal A, Deokar A, Mahajan S, Singh R, Bansal R, et al. Distinguishing features of acute Vogt-Koyanagi-Harada disease and acute central serous chorioretinopathy on optical coherence tomography angiography and en face optical coherence tomography imaging. Journal of Ophthalmic inflammation and infection. 2017;**7**(3). DOI: 10.1186/s12348-016-0122-z

[32] Aggarwal K, Agarwal A, Mahajan S, Invernizzi A, Mandadi SKR, Singh R, et al. The role of optical coherence tomography angiography in the diagnosis and management of acute Vogt-Koyanagi-Harada disease. Ocular Immunology and Inflammation. 2018;**26**(1):142-153

[33] Nussenblatt RB. Serpiginous choroidopathy. In: Nussenblatt RB, Whitcup SM, editors. Uveitis. Fundamentals and Clinical Practice. 4th ed. Vol. 2010. USA: Mosby. pp. 373-382

[34] Pakzad-Vaezi K, Khaksari K, Chu Z, Van Gelder RN, Wang RK, Pepple KL. Swept-source OCT angiography of serpiginous choroiditis. Ophthalmology Retina. 2018;**2**:712-719

[35] Ahn SJ, Park SH, Lee BR. Multimodal imaging including optical coherence tomography angiography in serpiginous choroiditis. Ocular Immunology and Inflammation. 2017;**25**(2):287-291

[36] El Ameen A, Herbort CP Jr. Serpiginous choroiditis imaged by optical coherence tomography angiography. Retinal Cases & Brief Reports. 2018;**12**(4):279-285

[37] Mandadi SKR, Agarwal A, Aggarwal K, Moharana B, Singh R, Sharma A, et al. Novel findings on optical coherence tomography angiography in patients with tubercular serpiginous-like choroiditis. Retina. 2017;**37**:1647-1659

[38] Amer R, Louis N. Punctate inner choroidopathy. Survey of Ophthalmology. 2011;**56**:36-53

[39] Essex RW, Wong J, Jampol LM, Dowler J, Bird AC. Idiopathic multifocal choroiditis: A comment on present and past nomenclature. Retina. 2013;**33**:1-4

[40] Spaide RF, Goldberg N, Freund KB. Redefining multifocal choroiditis and panuveitis and punctate inner choroidopathy through multimodal imaging. Retina. 2013;**33**:1315-1324

[41] Zahid S, Chen KC, Jung JJ, Balaratnasingam C, Ghadiali Q, Sorenson J, et al. Optical coherence tomography angiography of chorioretinal lesions due to idiopathic multifocal choroiditis. Retina. 2017;**37**:1451-1463

[42] Nussenblatt RB. White-dot syndromes. In: Nussenblatt RB, Whitcup SM, editors. Uveitis. Fundamentals and Clinical Practice. 4th ed. Vol. 2010. USA: Mosby. pp. 383-400

[43] Patel KH, Birnbaum AD, Tessler HH, Goldstein DA. Presentation and outcome of patients with punctate inner choroidopathy at a tertiary referral center. Retina. 2011;**31**:1387-1391

[44] Campos J, Campos A, Mendes S, Neves A, Beselga D, Sousa JPC. Punctate inner choroidopathy: A systematic review. Medical Hypothesis, Discovery & Innovation Ophthalmology. 2014; **3**(3):76-82

[45] Belfort R Jr, Silveira C, Muccioli C. Ocular toxoplasmosis. In: Ryan SJ, editor.

Retina. 6th ed. Philadelphia: Saunders; 2018. pp. 1681-1684

[46] Oréfice JL, Costa RA, Campos W, Calucci D, Scott IU, Oréfice F. Third-generation optical coherence tomography findings in punctate retinal toxoplasmosis. American Journal of Ophthalmology. 2006;**142**